J Mol Model (2012) 18:3147–3152
DOI 10.1007/s00894-011-1330-y

ORIGINAL PAPER

# Dynamical probing of allosteric control in nuclear receptors

**Mark A. Cunningham**

Received: 1 September 2011 / Accepted: 8 December 2011 / Published online: 6 January 2012


**Abstract** The dynamical behavior of the nuclear receptor LXR/RXR heterodimer was investigated with molecular dynamics simulations. The simulations reveal correlated motion between residues across the dimer interface that depends significantly on occupation of the ligand binding sites of the monomers. These results are broadly consistent with the observed experimental behavior of the dimers, where structural perturbation is thought to be a key element in signal transduction. Our results provide dynamical support for this model of allosteric control.

**Keywords** Nuclear receptor · LXR/RXR · Molecular · Dynamics

## Introduction

Nuclear receptors are a family of proteins that form a significant component of the transcriptional machinery regulating gene expression [9]. The receptors bind specific ligands, resulting in conformational shifts in the three-dimensional structure of the protein that provide signals for up- or down-regulating gene expression. The liver X receptors (LXR) recognize oxysterol ligands and form heterodimers with 9-cis retinoic acid receptors (RXR) [8]. The LXR/RXR heterodimer is illustrated in Fig. 1, which is taken from PDB ID 1UHL. The LXR monomer forms a bundle of 10 $\alpha$ helices; the RXR monomer forms a bundle of 11 $\alpha$ helices.

M. A. Cunningham (✉)
Department of Physics and Geology,
University of Texas-Pan American ,
SCIE 3.136 1201 West University Drive,
Edinburg, TX 78539-2999, USA
e-mail: cunningham@utpa.edu

*N*-(4-(1,1,1,3,3,3-hexafluoro-2-hydroxypropan-2-yl) phenyl)-*N*-(2,2,2-trifluoroethyl) benzenesulfonamide (TD-0901317; Cayman Chemical, Denver, CO) is the ligand for the LXR subunit and is depicted in the upper right-hand corner of the figure and, as a space-filling representation, in the ligand binding site of LXR. The ligand for the RXR subunit is (*S*, 2*E*, 4*E*)-11-methoxy-3,7,11-trimethyldodeca-2,4-dienoic acid (MEI), which is illustrated in the bottom corner of the figure and also shown in the binding site of RXR.

Information about the occupancy of the binding sites is conveyed through interactions of side chains of the two prominent $\alpha$ helices along the dimer interface [10]. The LXR/RXR heterodimers have been identified as key regulators of cholesterol homeostasis [13, 16] and are implicated in human metabolic diseases like atherosclerosis and diabetes [12]. So, developing a deeper understanding of the functioning of these molecules can lead to improvements in clinical practice.

This system has been the target of significant investigations and, to date, more than a dozen structures of LXR have been deposited in the PDB, with various ligands and some in complexes with RXR. Lacking, of course, in these structures is an assessment of the dynamics of the complexes, with and without ligands. Here, we report the results of our investigations of the LXR/RXR system using molecular dynamics as a probe of the mechanistic aspects of signalling.

## Methods

Molecular dynamics simulations were performed with the program NAMD [6], using the CHARMM 27 force field parameters [7]. The LXR/RXR model was prepared from PDB ID 1UHL. Parameters for ligand molecules were obtained by analogy to similar chemical moieties within

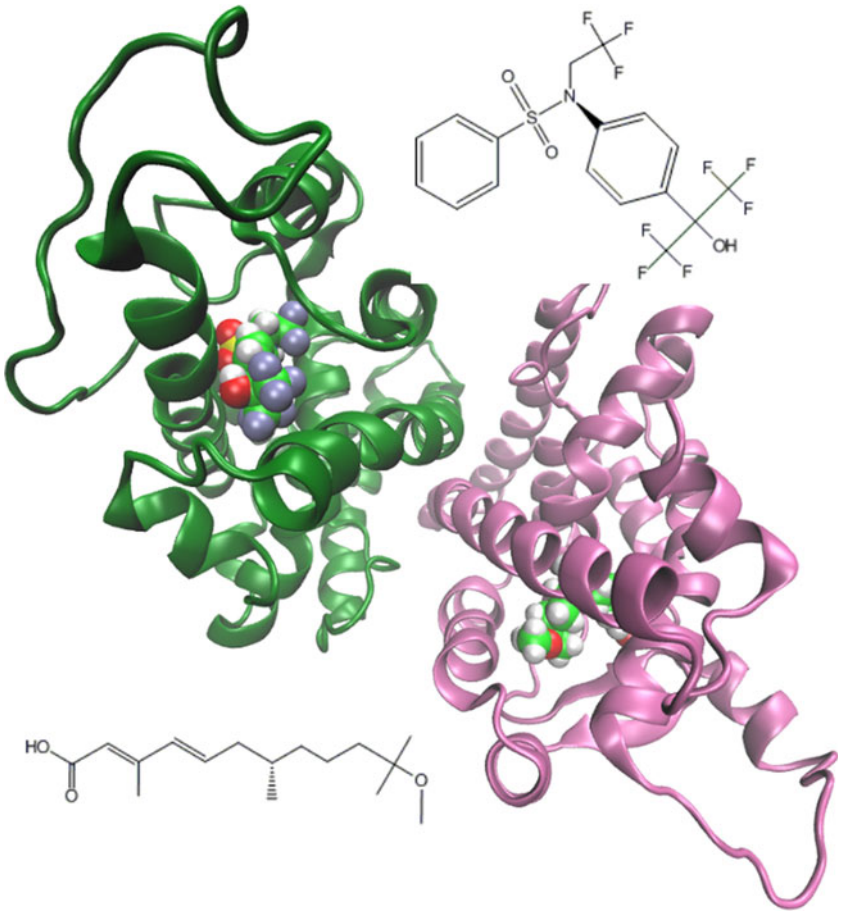


**Fig. 1** Liver X receptor/retinoic acid receptor (LXR/RXR) heterodimer. The LXR (*dark green*) and RXR (*mauve*) monomers are illustrated with a cartoon representation and interact via residues on the helices along the dimer interface. The ligands are depicted in a space-filling representation: *green* carbon atoms, *red* oxygen atoms, *white* hydrogen atoms, *yellow* sulfur atoms, *light blue* fluorine atoms. The ligands are also shown as *line drawings*

the CHARMM force field. That is, the atom types for the ligand were defined to be types already existing within the CHARMM 27 parameterization. Residue definitions within the topology file were constructed by hand and parameters chosen from similar moieties. For example, the (unprotonated) carboxyl group of MEI shares the same atom types and parameters as the carboxyl from either the aspartate or glutamate residues that are found in the amino acid parameterizations.

Analysis of the simulation results was conducted with the program VMD [5], which was also used to draw the molecular representations. Molecular line drawing were produced with the program ChemBioDraw 11 ® (CambridgeSoft, Cambridge, MA). Simulation models were constructed from the original crystal structures using the PSFGEN utility of NAMD. Histidine residues were singly protonated, using likely hydrogen bonding conformations from the crystal structure as a guide for choosing between protonating the N$\delta$ nitrogen atom or the N$\varepsilon$ nitrogen atom; all hydrogen atoms were placed using PSFGEN. The models were solvated with a buffer of TIP3 water for 10 Å surrounding the protein. After the equilibration process described below, we found that this resulted in a 7–8 Å water buffer, ensuring that the models represent a diffuse limit in which protein atoms do not interact with other protein atoms in periodic images, given the 10 Å cutoff used for electrostatic interactions. The total electric charge of each model was set to zero by replacing the requisite number of water molecules with sodium ions. In cases where mutations or ligand deletions resulted in a charge change from the base model, an additional ion was added to neutralize the charge. Model systems typically incorporated about 60,000 atoms.

Simulations were conducted at 300 K and began with a small number of minimization steps (500–1,000), followed by about 10,000 steps of dynamics, all with the protein and ligands restrained harmonically. Periodic boundary conditions were employed throughout, as was the particle-mesh Ewald method for electrostatics [1]; SHAKE [14] was used to constrain hydrogen atoms. An additional 50 ps of constant volume (NVT) dynamics was conducted with a time step of 1 fs to further equilibrate the system. The harmonic constraints were then removed from the protein and ligand and the models equilibrated for another 50 ps, using 1 fs time steps and enforcing constant pressure (NPT) using a Langevin piston Nose-Hoover technique. [2–4]. Trajectory data from NPT production runs, utilizing 2 fs time steps,

were written to disk every picosecond of the simulation; simulations were conducted for total times in excess of 40 ns.

Trajectories were analyzed using the program VMD using the final 40 ns (40,000 samples) of the simulation data. We computed average structures for comparison with experimental structures. We also computed cross-correlation matrices $M$ for the dynamics runs. At each time step along the trajectory, the change in the center-of-mass position $\Delta x_i$ was computed for each residue $i$. The cross-correlation matrix elements were constructed as follows:

$$M_{ij} = \frac{1}{N} \sum \frac{\Delta x_i \cdot \Delta x_j}{|\Delta x_i||\Delta x_j|},$$

where the summation extends over all $N$ frames in the trajectory. Plots of the matrix elements were produced in the program MatLab ® from the Mathworks (Natick, MA).

## Results and discussion

Our initial simulations were conducted with the LXR/RXR dimer, with both ligand binding sites occupied and with two short peptide helical segments (chains C and D) found in the 1UHL structure. We also performed simulations without the peptide fragments and found no significant differences in the results (data not shown). The peptide fragments are important for crystallization of the protein but do not appear to affect the interactions at the LXR/RXR interface. The average structure obtained from the final 20 ns portion of the trajectory is compared to the 1UHL experimental structure in Fig. 2. We observe a 1.85 Å RMS difference between the structures for Cα carbon atoms of the LXR and RXR subunits. Visually, these differences are manifested primarily in differences in flexible loops away from the dimer interface; we suggest that the observed differences are due principally to crystal packing forces that are not present in our "diffuse limit" simulations. We see no significant differences between the average structures obtained from either the initial or final 20 ns of the trajectory in the area of the LXR/RXR interface. The 1.3 Å RMS difference between the average structures from the beginning and end of the trajectory again is due to flexible loops away from the dimer interface.

Figure 3 shows the correlation matrix obtained from the simulation with both ligands present. The diagonal elements are unity, as expected and as indicated by the white diagonal line. We observe significant matrix elements within each of the LXR and RXR subunits. We infer that this is indicative of persistent interactions within the monomers. The correlation matrix serves as something of a dynamical fingerprint, identifying persistent interactions between residues in the protein. After trying different strategies for visualizing the matrix elements, we settled upon the format in which negative (anti-correlated motion) matrix elements were plotted in the lower half of the matrix and positive matrix elements (correlated motion) in the upper half. We see no particular evidence for anti-correlated motion in Fig. 3 and, indeed, in the other simulations that we have conducted for this system. We can now examine the results of conducting simulations without ligands present in the binding sites. Model building proceeded as described above; models were constructed with (1) only MEI in the RXR binding site, (2) only

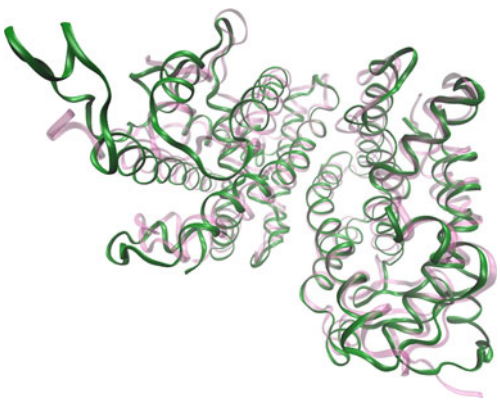

**Fig. 2** Average structure. The average structure obtained over the final 20 ns of a 44 ns trajectory is depicted as the *dark green ribbon* diagram. The 1UHL crystal structure is depicted in *mauve*

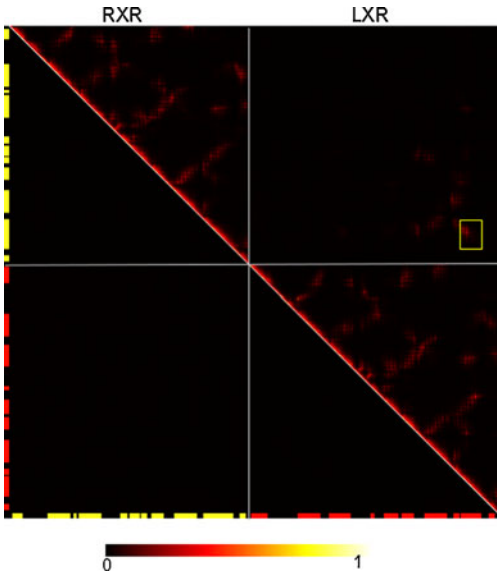


**Fig. 3** Correlation matrix. The matrix elements $M_{ij}$ are colored according to the scale bar shown at the bottom of the plot. The *red* and *yellow blocks* at the border of the image mark locations of the helices in RXR and LXR, respectively. Positive matrix elements are illustrated in the upper half of the matrix and negative matrix elements are illustrated in the lower half. Matrix elements within the *yellow square* indicate interactions between the two helices at the RXR/LXR interface.

TD-0901317 in the LXR binding site and (3) neither ligand. Correlation matrices were computed as described above. To compare the results directly, we converted the image resulting from simulation (1) with no LXR ligand, mapping the red channel into green. (The resulting image looks much like Fig. 3 but green.) We then add the two images to produce the result displayed in Fig. 4. Here, interactions that are present in both simulations will be yellow. Interactions present when both ligands are present will appear red, and interactions present when only the RXR ligand is bound will appear green.

We observe a number of red spots in the lower portion of the upper triangular region of the image: these correspond to persistent interactions present in the LXR subunit that arise upon binding of ligand. There are also some changes (green spots) in the leftmost portion of the upper triangular region of the image: these correspond to persistent interactions within the RXR subunit that are lost upon binding of the LXR ligand. We also observe a number of changes in the upper quadrant of the image: these correspond to changes in the interactions between the RXR and LXR monomers.

To illustrate how these interactions map to the structure, in Fig. 5, we have drawn lines between the Cα carbon atoms of residues where the matrix element exceeds a threshold value of 0.3. Interactions that are present in the simulation with both ligands and in the simulation with only the RXR ligand are drawn as dark orange lines. Interactions present in the simulation with both ligands are drawn in red. Interactions present when only the RXR ligand is bound are drawn in green. We observe that the secondary structures of each of the LXR and RXR subunits are connected strongly in this representation, confirming that the interactions among the residues that make up the helices are persistent. We also observe correlations between the two helices across the dimer interface that change when the LXR ligand is also bound. The persistent interactions in the center of the helix are lost, and there is a shift in the binding of the N-terminal portion of helix 9 in LXR. In particular, there is an interaction between Arg401 of LXR and Glu465 of RXR that arises when both ligands are present. Without the LXR ligand, Arg401 forms a persistent interaction with Glu472 of RXR, suggesting a significant shift in registration of the helices upon LXR ligand binding.

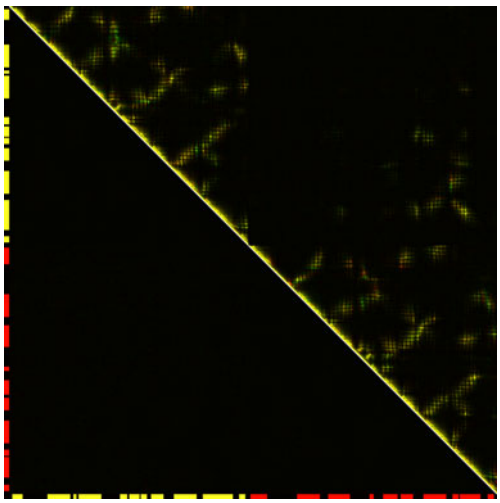

**Fig. 4** Correlation comparison for loss of LXR ligand. The correlation matrix for the simulation with only the RXR ligand (*green*) is added to the matrix for both ligands (*red*). Matrix elements that are yellow indicate interactions present for both simulations. The bars at the border indicate helix positions in the RXR and LXR subunits, as in Fig. 3

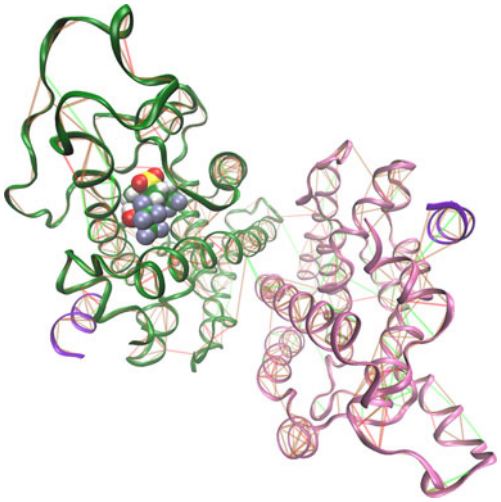

**Fig. 5** LXR/RXR heterodimer correlated motion. The LXR (*dark green*) and RXR (*mauve*) monomers are depicted as *ribbons*, along with small helical segments (*blue*). The RXR ligand (TD-0901317) is depicted in a space-filling representation with the same color scheme as in Fig. 1. *Lines* connect Cα carbon atoms where the cross-correlation matrix elements exceed a threshold of 0.3. *Red lines* indicate the interaction was present only in the simulation with both ligands. *Green lines* indicate the interaction was present only in the simulation with the RXR ligand. *Dark orange lines* indicate the interaction was present in both simulations

If we now examine the results of comparing our base simulation with both ligands present with simulation (2) in which only the LXR ligand is present, we can assess the changes due to loss of the RXR ligand. In Fig. 6, we depict the correlated motion as in Fig. 5. Here we observe interactions between the dimers along the RXR/LXR interface that are modified upon binding of the RXR ligand. As in Fig. 5, we see that there is a significant shift in the interactions at the N-terminal end of helix 9 of LXR, corresponding to the realignment of the Arg401 residue from LXR. In the center of helix 9 of LXR, we observe interactions of Arg415 of LXR with Pro494 and Ser498 from RXR (green lines) that are lost upon ligand binding. We can infer that the loss of flexibility of the helix due to ligand binding reduces those interactions to a more intermittent status.

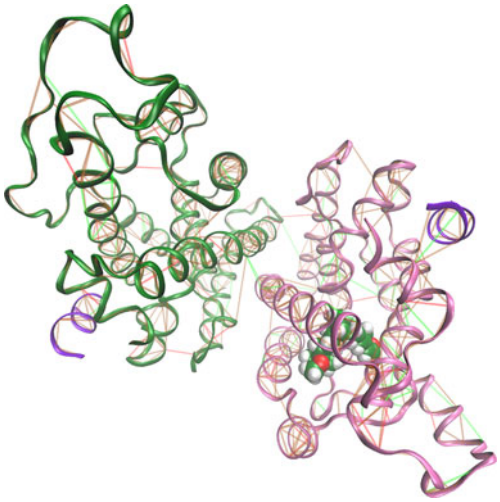

**Fig. 6** Correlation comparison for loss of RXR ligand. Coloring is the same as in Fig. 5. Here only the LXR ligand [(*S*, 2*E*, 4*E*)-11-methoxy-3,7,11-trimethyldodeca-2,4-dienoic acid (MEI)] is depicted

Previous molecular dynamics simulations in this system [15] pointed to differences in interaction energies between the helices when ligands were bound. Additionally, different ligands led to different interaction energies. Overall, the effects of ligand binding was attributed to changes in the hydrogen-bonding network and not to changes in the hydrophobic interactions between the helices. Our analysis provides a somewhat different perspective but we also find that the interaction patterns shift when ligands are bound. We have not explicitly examined the results of different ligands in this work but our analysis of correlated motion must, of course, reflect the hydrogen-bonding network that provides the overall structure of the model.

If we now look at correlated motion in simulation (3) with no ligands, that we illustrate in Fig. 7, we see that the Arg401 residue of LXR interacts with the Glu465 residue of RXR, as was the case for the simulation with both ligands present. In this case, however, there are persistent interactions in the apo simulation (3) that are not present when both ligands are bound.

Our simulations suggest that persistent interactions within each of the subunits are modified when either ligand is bound. We can infer, not surprisingly, that this observation reflects the additional rigidity provided by the ligand-protein hydrogen bonding interactions within the subunit. In our analysis, this is accomplished without specific reference to particular hydrogen bonds and is therefore insensitive to some of the analytical complexities associated with tracking hydrogen bonds. (For example, the equivalent carboxyl oxygen atoms of an aspartate or glutamate may exchange positions during a simulation and still maintain a persistent bond to a neighboring lysine residue.) By studying only the center-of-mass motion, our analysis is less sensitive to such details.

Examination of Figs. 5, 6 and 7 generally indicate that there are a number of interactions between the two helices at the LXR/RXR interface that are lost when the ligands bind (red lines). In addition, the persistent interaction at the N-terminal end of helix 9 of LXR due to the Arg401 residue, shifts depending upon the binding site occupation. This provides us with a hint that, at much longer time scales, a conformational shift may arise that would lead to the sort of allosteric control that is presumed to underlie the action of the nuclear receptors[11]. Certainly, our results suggest that mutations in the LXR residue Arg401 and/or the RXR residues Glu465 and Glu472 should be investigated as this is the particular interaction that arises upon both ligands binding.

## Summary

The nuclear receptor superfamily provides fertile ground for supporting laboratory experimentation with numerical experimentation to provide additional, dynamical perspectives on protein mechanisms. Signal transduction via ligand binding is a complex process that depends subtly but significantly on interactions between residues within the protein. We have demonstrated that numerical simulation provides another window into the processes that govern the conformational shifts experienced by the receptors and that there is broad, if not detailed, agreement with experimental observations. We have observed a shift in the interactions of Arg401 of the LXR subunit due to ligand binding and this should be verifiable experimentally. A valid criticism of this approach is that it remains difficult to extend the calculations into the

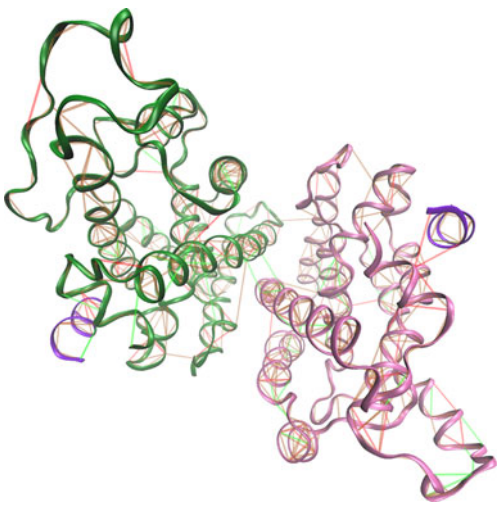

**Fig. 7** Correlation comparison for loss of both ligands. Coloring is the same as in Fig. 5

millisecond or second time scales that would make more direct contact with experimental measurements possible. Nevertheless, the modest calculations reported here do reflect the differences observed in the heterodimer behavior with and without ligands bound. The simulations can, even at this level of sophistication, provide useful insights into the transcriptional machinery.

**Acknowledgments** The author would like to thank Kendall Nettles at Scripps Florida for providing the motivation to undertake this work. This project was supported in part through the National Science Foundations FaST program (HRD-0703584), administered by the Department of Educational Programs at Argonne National Laboratory. The author acknowledges the Texas Advanced Computing Center (TACC) at The University of Texas at Austin for providing HPC resources that have contributed to the research results reported within this paper. URL: http://www.tacc.utexas.edu

## References

1. Essmann U, Perera L, Berkowitz ML, Darden T, Lee H, Pedersen LG (1995) A smooth particle mesh ewald method. J Chem Phys 103(19):8577–8593, doi: 10.1063/1.470117, URL http://link.aip.org/link/?JCP/103/8577/1
2. Feller SE, Zhang Y, Pastor RW, Brooks BR (1995) Constant pressure molecular dynamics simulation: The langevin piston method. The Journal of Chemical Physics 103(11):4613–4621, doi: 10.1063/1.470648, http://link.aip.org/link/?JCP/103/4613/1
3. Hoover WG (1985) Canonical dynamics: equilibrium phase-space distributions. Phys Rev A 31(3):1695–1697. doi:10.1103/PhysRevA.31.1695
4. Hoover WG (1986) Constant-pressure equations of motion. Phys Rev A 34(3):2499–2500. doi:10.1103/PhysRevA.34.2499
5. Humphrey W, Dalke A, Schulten K (1996) VMD—Visual Molecular Dynamics. J Mol Graphics 14:33–38
6. Kalé L, Skeel R, Bhandarkar M, Brunner R, Gursoy A, Krawetz N, Phillips J, Shinozaki A, Varadarajan K, Schulten K (2002) NAMD2: Greater scalability for parallel molecular dynamics. J Comput Phys 9:646–652
7. MacKerell AD Jr, Bashford D, Bellott M, Evanseck RLDJJ, Field MJ, Fischer S, Gao J, Guo H, Ha S, Joseph D, Kuchnir L, Kuczera K, Lau FTK, Mattos C, Michnick S, Ngo T, Nguyen DT, Prodhom B, Reiher WE III, Roux B, Schlenkrich M, Smith J, Stote R, Straub J, Watanabe M, Wiorkiewicz-Kuczera J, Yin D, Karplus M (1998) All-atom empirical potential for molecular modeling and dynamics studies of protein. J Phys Chem B 102:3586–3616
8. Mangelsdorf DJ, Thummel C, Beato M, Herrlich P, Schtz G, Umesono K, Blumberg B, Kastner P, Mark M, Chambon P, Evans RM (1995) The nuclear receptor superfamily: The second decade. Cell 83(6):835–839. doi:DOI: 10.1016/0092-8674(95)90199-X, URL
9. McEwan IJ (2009) Nuclear receptors: One big family. In: McEwan IJ, Walker JM (eds) The nuclear receptor superfamily. Methods in molecular biology, vol 505, Humana Press, pp 3–18, http://dx.doi.org/10.1007/978-1-60327-575-0 doi:10.1007/978-1-60327-575-0_1
10. Nettles KW, Greene GL (2005) Ligand control of coregulator recruitment to nuclear receptors. Annu Rev Physiol 67(1):309–333, doi:10.1146/annurev.physiol.66.032802.154710, http://www.annualreviews.org/doi/abs/10.1146/annurev.physiol.66.032802.154710, http://www.annualreviews.org/doi/pdf/10.1146/annurev.physiol.66.032802.154710
11. Nettles KW, Sun J, Radek JT, Sheng S, Rodriguez AL, Katzenellenbogen JA, Katzenellenbogen BS, Greene GL (2004) Allosteric control of ligand selectivity between estrogen receptors [alpha] and [beta]: Implications for other nuclear receptors. Mol Cell 13(3):317 – 327, doi:10.1016/S1097-2765(04)00054-1, http://www.sciencedirect.com/science/article/pii/S1097276504000541
12. Oosterveer MH, Grefhorst A, Groen AK, Kuipers F (2010) The liver x receptor. Control of cellular lipid homeostasis and beyond: implications for drug design. Prog Lipid Res 49(4):343–352, doi:10.1016/j.plipres.2010.03.002, http://www.sciencedirect.com/science/article/pii/S0163782710000172
13. Repa JJ, Turley SD, Lobaccaro JMA, Medina J, Li L, Lustig K, Shan B, Heyman RA, Dietschy JM, Mangelsdorf DJ (2000) Regulation of absorption and abc1-mediated efflux of cholesterol by rxr heterodimers. Science 289(5484):1524–1529, doi:10.1126/science.289.5484.1524, http://www.sciencemag.org/content/289/5484/1524.abstract, http://www.sciencemag.org/content/289/5484/1524.full.pdf
14. Ryckaert JP, Ciccotti G, Berendsen HJC (1977) Numerical integration of the cartesian equations of motion of a system with constraints: molecular dynamics of n-alkanes. J Comput Phys 23 (3):327–341, doi:10.1016/0021-9991(77)90098-5, http://www.sciencedirect.com/science/article/pii/0021999177900985
15. Yue L, Ye F, Gui C, Luo H, Cai J, Shen J, Chen K, Shen X, Jiang H (2005) Ligand-binding regulation of lxr/rxr and lxr/ppar heterodimerizations: Spr technology-based kinetic analysis correlated with molecular dynamics simulation. Protein Sci 14(3):812–822, doi:10.1110/ps.04951405, http://dx.doi.org/10.1110/ps.04951405
16. Zelcer N, Hong C, Boyadjian R, Tontonoz P (2009) Lxr regulates cholesterol uptake through idol-dependent ubiquitination of the ldl receptor. Science 325(5936):100–104, doi:10.1126/science.1168974, http://www.sciencemag.org/content/325/5936/100.abstract, http://www.sciencemag.org/content/325/5936/100.full.pdf